

Ultracold Atoms in a Square Lattice with Spin-Orbit Coupling: Charge Order, Superfluidity, and Topological Signatures

Peter Rosenberg, Hao Shi, and Shiwei Zhang

Department of Physics, The College of William and Mary, Williamsburg, Virginia 23187, USA

(Received 7 July 2017; published 28 December 2017)

We present an *ab initio*, numerically exact study of attractive fermions in square lattices with Rashba spin-orbit coupling. The ground state of this system is a supersolid, with coexisting charge and superfluid order. The superfluid is composed of both singlet and triplet pairs induced by spin-orbit coupling. We perform large-scale calculations using the auxiliary-field quantum Monte Carlo method to provide the first full, quantitative description of the charge, spin, and pairing properties of the system. In addition to characterizing the exotic physics, our results will serve as essential high-accuracy benchmarks for the intense theoretical and especially experimental efforts in ultracold atoms to realize and understand an expanding variety of quantum Hall and topological superconductor systems.

DOI: [10.1103/PhysRevLett.119.265301](https://doi.org/10.1103/PhysRevLett.119.265301)

Exotic states of matter, including high- T_c superconductivity and topological phases, have long been a focus of condensed matter physics. However, many of these behaviors are challenging to detect and characterize in real materials, where fixed structural and electromagnetic properties typically provide limited access to the parameter space. Modern cooling and trapping techniques in ultracold atoms, combined with optical lattice potentials [1,2] and artificial gauge fields [3–8], have opened a new window onto these novel phases, which can be explored across broad parameter regimes well beyond those available to experiments with real materials.

Ultracold atoms in optical lattices thus provide access to clean, tunable systems in which to study the combination of strong interactions and spin-orbit coupling (SOC) with extreme precision. These systems display a number of exotic phases. A thorough understanding, and high-accuracy characterization, of these phases will have important implications across the fields of spintronics and quantum computation and information [9–11], among others.

The importance of high-accuracy numerical benchmarks has grown considerably with the recent advent of Fermi gas microscopes, capable of performing site-resolved measurements of lattice fermions [12–16]. This expansive experimental horizon, and the promise of high-accuracy measurements of these disorder-free and finely tunable systems, has opened a new avenue to explore many open questions [17–21]. Complementary experimental and theoretical efforts will help shed light on the novel physics realized in these systems, which combine strong interaction, exotic pairing, and superconductivity, as well as topological effects.

Despite this rapidly growing interest, the ground-state properties of lattice fermions with attractive interactions and SOC, a candidate system for the realization of many

novel phases, remain largely uncharacterized. Calculations based on the mean-field theory [20,22,23] have indicated a variety of interesting phases. However, these approaches can be sensitive to the decomposition used and the corresponding symmetry-breaking terms. To reliably determine the ground state of a strongly interacting system with coexisting orders requires a highly accurate many-body approach. Many-fermion systems are notoriously challenging to treat theoretically or computationally. Applying several advances in auxiliary-field quantum Monte Carlo (AFQMC) simulations [24–26], including accelerated sampling [27] with force bias [28], control of Monte Carlo variance [29], and treatment of SOC [30], we show that systematic and high-precision numerical data can be obtained on the ground-state properties of this remarkable system [31]. The spin-balanced situation, when no Zeeman field is present, preserves time-reversal symmetry such that the calculations can be made free of the fermion sign problem [30,35], and the results here are unbiased and numerically exact. This work thus serves as an illustration of the power of state-of-the-art computational approaches for exotic, strongly correlated quantum systems, in a system which is on the verge of experimental realization.

Our results allow a quantitative description of attractive fermions with Rashba SOC in a two-dimensional (2D) optical lattice, which displays a supersolid phase [36–40] with both singlet and triplet pairing and topological signatures. We elucidate the unique pairing properties of the system and their connections to the spin and momentum distributions. The interplay between pairing and the charge order at half filling is characterized. Moreover, we examine the edge currents to explore the emergence of topological behavior, in the context of Majorana edge modes which are of strong current interest.

The Hamiltonian for ultracold fermions in a 2D optical lattice with Rashba SOC is written

$$\hat{H} = \sum_{\mathbf{k}\sigma} \varepsilon_{\mathbf{k}} c_{\mathbf{k}\sigma}^\dagger c_{\mathbf{k}\sigma} + \sum_{\mathbf{k}} (\mathcal{L}_{\mathbf{k}} c_{\mathbf{k}\downarrow}^\dagger c_{\mathbf{k}\uparrow} + \text{H.c.}) + \sum_i U n_{i\uparrow} n_{i\downarrow}, \quad (1)$$

with $\varepsilon_{\mathbf{k}} = -2t(\cos k_x + \cos k_y)$ and $\mathcal{L}_{\mathbf{k}} = 2\lambda(\sin k_y - i \sin k_x)$. The parameter t , set to unity throughout this work, determines the strength of nearest-neighbor hopping, the parameter λ controls the strength of the SOC, and the parameter U (< 0) determines the strength of the on-site attractive interaction, with $n_{i\sigma} = c_{i\sigma}^\dagger c_{i\sigma}$ denoting the density operator in real space on site i with spin σ ($= \uparrow$ or \downarrow). We will focus mostly on half filling in this work, with a total number of atoms equal to the number of lattice sites.

Although the existence and stability of a supersolid (superconducting charge-density-wave) state in the attractive Hubbard model has been well understood [39,40], the properties of this phase in the presence of Rashba SOC remain largely uncharacterized. Here we provide a precise characterization of this phase and study its properties and their interplay with SOC strength. We examine the charge order by measuring the density-density correlation function $D(i, j) = \langle n_i n_j \rangle$, with $n_i = (n_{i\uparrow} + n_{i\downarrow})$. (Expectation values denoted by angle brackets are always taken with respect to the many-body ground state in this work.) Several quantities are measured to probe superfluidity, including the s -wave pair-pair correlation $P_{1s}(i, j) = \langle \Delta_i^\dagger \Delta_j \rangle$, where $\Delta_i^\dagger = c_{i\uparrow}^\dagger c_{i\downarrow}^\dagger$ creates a singlet pair at lattice site i . In periodic supercells, we average over the reference site j and will label it as “0” for convenience.

A characteristic example of the supersolid state is shown in Fig. 1. Plotted in the upper left corner is the density-density correlation function, which provides an illustration of the charge-density wave (CDW). A clear checkerboard pattern is seen, with a persistent alternating order. Sites that belong to the same sublattice as the reference have above-average occupation, while those on the other sublattice have below-average occupation. The amplitude of the CDW is essentially constant across the lattice. We have verified with calculations on larger supercell sizes that the long-range values of the CDW is independent of size, providing strong evidence of long-range order. Plotted below the density-density correlation is the pair-pair correlation function. In this case, the presence of long-range superfluid order is evident from the significant magnitude of the pair-pair correlation across the lattice.

The effects of increasing SOC strength on these correlations are illustrated in the right column in Fig. 1, which shows slices of the density-density correlation in the top panel and the pair-pair correlation in the bottom panel. The correlations evolve in equal proportion to each other with increasing SOC, which is a reflection of the underlying particle-hole symmetry. For small values of λ , the supersolid state is robust, with charge and superfluid orders of sizable magnitude. As SOC increases, these orders are

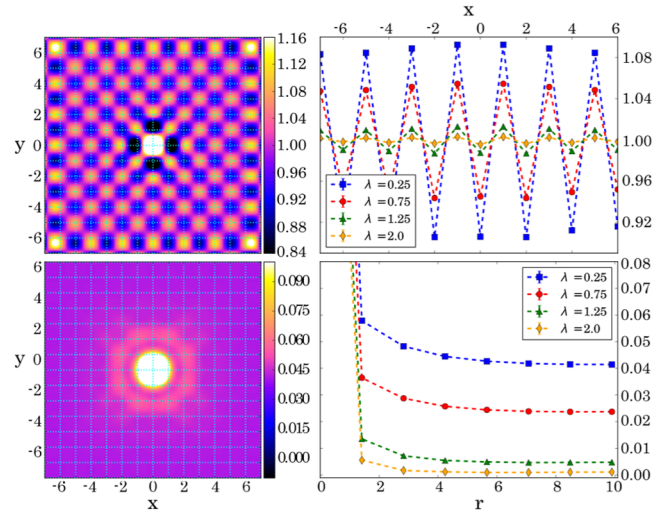


FIG. 1. Density-density (upper panel) and pair-pair (lower panel) correlation functions. The left column is for one SOC strength $\lambda = 0.25$, while the right column shows the evolution for i running through the entire periodic supercell (14×14). The upper right panel shows $D(i, 0)$ for a slice of sites i along $i_y = -3$, while the lower right panel shows $P_{1s}(i, 0)$ for a slice along the diagonal, $i_x = i_y$.

diminished. However, even at strong SOC, such as $\lambda = 2.0$, both remain finite.

The nature of pairing is altered in a fundamental way by the presence of SOC. The singlet and triplet channels are mixed, resulting in a pair wave function with both singlet and triplet components, $\Psi_p = \psi_p^s + \psi_p^t$. We investigate pairing via the construction and diagonalization of the two-body density matrix in momentum space:

$$\rho_2(\mathbf{k}, \chi; \mathbf{q}, \chi') = \langle \Delta_\chi^\dagger(\mathbf{k}) \Delta_{\chi'}(\mathbf{q}) \rangle, \quad (2)$$

with $\chi = s$ or t_\uparrow or t_\downarrow . The singlet and triplet pairing operators are

$$\begin{aligned} \Delta_s^\dagger &= \frac{1}{\sqrt{2}} (c_{\mathbf{k}\uparrow}^\dagger c_{-\mathbf{k}\downarrow}^\dagger - c_{\mathbf{k}\downarrow}^\dagger c_{-\mathbf{k}\uparrow}^\dagger), \\ \Delta_{t_\uparrow}^\dagger &= c_{\mathbf{k}\uparrow}^\dagger c_{-\mathbf{k}\uparrow}^\dagger, \\ \Delta_{t_\downarrow}^\dagger &= c_{\mathbf{k}\downarrow}^\dagger c_{-\mathbf{k}\downarrow}^\dagger, \end{aligned} \quad (3)$$

while the third component of the triplet pairing vanishes by symmetry. The leading eigenvalue, N_c , of the $3N \times 3N$ matrix ρ_2 gives the condensate fraction of the pairs [41]: $n_c \equiv N_c/N$. The corresponding eigenstate gives the pair wave function.

The structures of the pair wave functions, $\psi_p^s(\mathbf{k})$ and $\psi_p^t(\mathbf{k})$, are illustrated in Fig. 2. To better understand their physical origin, we also compute the momentum distributions, which are shown in the left panel. At each \mathbf{k} , the total occupancy is given by $\langle n_{\mathbf{k}} \rangle = \langle c_{\mathbf{k}\uparrow}^\dagger c_{\mathbf{k}\uparrow} + c_{\mathbf{k}\downarrow}^\dagger c_{\mathbf{k}\downarrow} \rangle$.

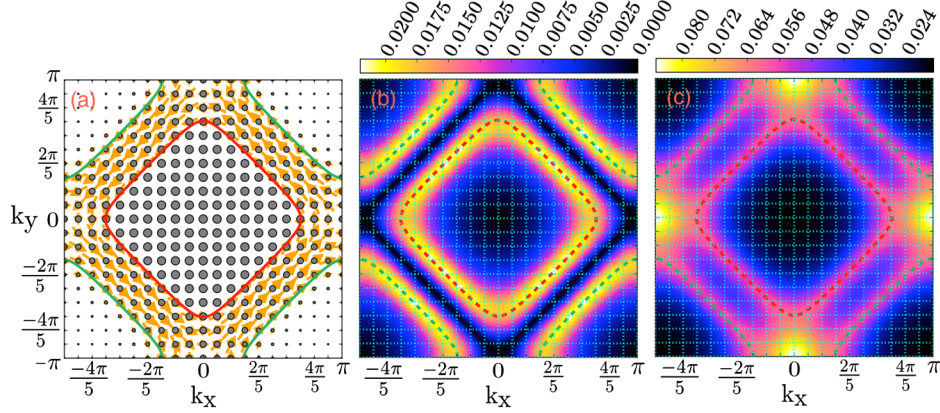


FIG. 2. Spin distribution and momentum-space pair wave functions. In (a), the arrow length and direction give the magnitude and orientation of the spin expectation, respectively, at each lattice momentum, and the dot size is proportional to the total occupation. The amplitude of the triplet and singlet parts of the pairing wave function are plotted in (b) and (c), respectively, with the noninteracting Fermi surfaces indicated by the dashed curves. The system is a 20×20 periodic supercell.

The expectations of the spin components are $\langle S_{\mathbf{k}}^x \rangle = \langle c_{\mathbf{k}\uparrow}^\dagger c_{\mathbf{k}\downarrow} + c_{\mathbf{k}\downarrow}^\dagger c_{\mathbf{k}\uparrow} \rangle / 2$ and $\langle S_{\mathbf{k}}^y \rangle = \langle c_{\mathbf{k}\uparrow}^\dagger c_{\mathbf{k}\downarrow} - c_{\mathbf{k}\downarrow}^\dagger c_{\mathbf{k}\uparrow} \rangle / 2i$, with $\langle S_{\mathbf{k}}^z \rangle = 0$ by symmetry here. Thus, the magnitude and orientation of $\langle S_{\mathbf{k}} \rangle$ can be determined. In addition, the noninteracting Fermi surfaces are shown in the figure for reference, which are easily obtained from the two helicity branches of the dispersion relations, $\epsilon_{\mathbf{k}}^\pm = -2t(\cos k_x + \cos k_y) \pm 2\lambda\sqrt{\sin^2 k_x + \sin^2 k_y}$.

The pair wave functions illustrate that triplet pairing occurs across the entirety of both Fermi surfaces (one for each helicity band). Singlet pairing also occurs across both Fermi surfaces, but with SOC it becomes strongly peaked near the four band-touching points, which occur at the half filling Fermi level at $\mathbf{k} = (\pm\pi, 0), (0, \pm\pi)$. As indicated by the spin and momentum distributions, these points have no excess spin but are not fully occupied. They are also the only points in momentum space that are surrounded by almost antiparallel spins. The excitation of these neighboring antiparallel spins into the momentum states at the band-touching points dramatically promotes singlet pairing across the Fermi surface at these points.

Figure 3 plots, as a function of the SOC strength, the behavior of the pair wave functions in real space, which are given by the Fourier transforms of $\psi_p^s(\mathbf{k})$ and $\psi_p^t(\mathbf{k})$. For small values of SOC, the singlet pair wave function (right column) closely resembles the pair wave function in the absence of SOC, with a large well-localized peak indicating strong on-site pairs. However, at increasing values of the SOC strength, the amplitude of the central peak is reduced and the pair wave function becomes less strongly localized. At large λ , this delocalization is evident from the development of additional peaks in the singlet pair wave function away from the origin.

The triplet pair wave function at small values of SOC shows several peaks along both diagonals, with the

strongest amplitudes located at the second-nearest-neighbor sites to the origin. As the SOC strength increases, the amplitude of the pair wave function grows at the third-nearest-neighbor sites, finally displaying an intriguing diamond pattern of peaks at the second- and third-nearest-neighbor sites for large SOC strengths. This

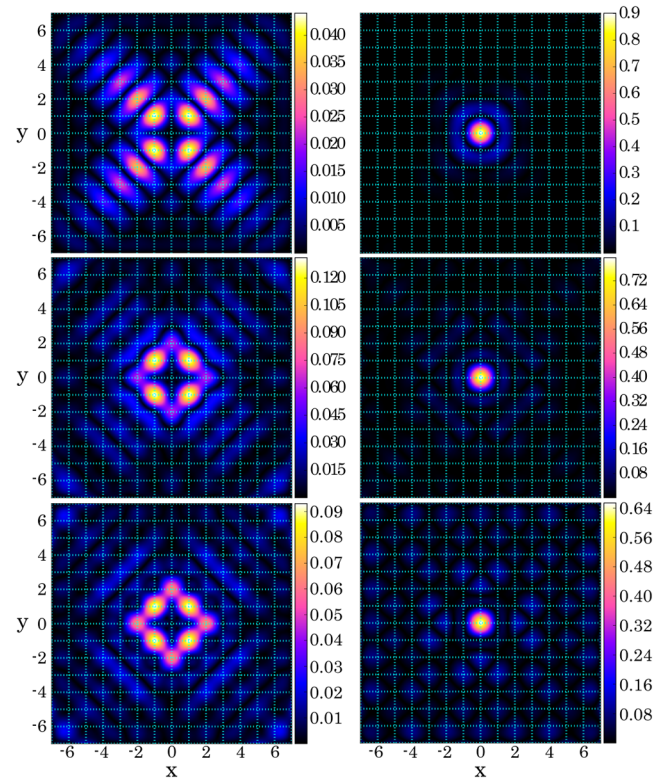


FIG. 3. Triplet (left) and singlet (right) pair wave functions in real space. From top to bottom, $\lambda = 0.25, 1.0, 1.5$. The interaction strength is $U/t = -4$, and the system is a 14×14 periodic supercell.

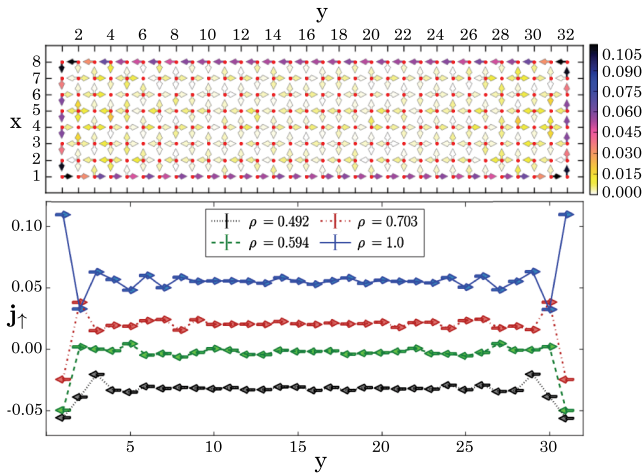


FIG. 4. Edge current in the open system. The top panel shows the edge current at half filling for spin \uparrow , with the direction and magnitude of the current indicated by the arrow direction and its color. The bottom panel illustrates the evolution of the current with doping, plotting the current in the y direction versus y at $x = 1$.

structure is a consequence of the spin-flipping process introduced by the presence of SOC, which implies that, for a given spin at the origin, a parallel spin can be found two nearest-neighbor sites away as a result of successive hops accompanied by spin flips.

The potential realization of nontrivial topological and pairing states, with exotic spin transport properties, makes this system particularly compelling. Given that the presence of persistent, topologically protected edge modes is an important first step towards reliable spintronic devices and quantum computation, a high-accuracy numerical treatment of these behaviors is essential. We examine the existence and behavior of edge currents in the system with open boundary conditions. We have verified by comparing multiple calculations with periodic and open boundary conditions that the other properties discussed so far remain consistent. In a system with open boundaries, we compute the spin current operator

$$\mathbf{j}_{nm,\sigma} = -it(c_{m\sigma}^\dagger c_{n\sigma} - c_{n\sigma}^\dagger c_{m\sigma}), \quad (4)$$

which provides a measure of the current for spin- σ particles between sites n and m . The top row in Fig. 4 plots $\mathbf{j}_{nm,\uparrow}$ for $\lambda = 2.0$ and clearly establishes the presence of a spin current along the boundaries of the system. The strength of this edge current increases monotonically with increasing SOC. The current for spin \downarrow is of equal magnitude and opposite direction, as required by time-reversal symmetry, such that the net current vanishes in this system.

While the present study is focused on the spin-balanced system at half filling, it has been suggested [11,42,43] that, with the introduction of a time-reversal-symmetry-breaking Zeeman field and appropriate parameters, this system may host Majorana fermions. Mean-field calculations at half

filling indicate that the presence of a Zeeman field, even of considerable magnitude, is not sufficient to create spin- \uparrow and spin- \downarrow currents of different magnitude, and the system remains in a state with Chern number $0, \pm 2$ [43]. For doped systems, mean-field studies suggest that the spin- \uparrow and spin- \downarrow currents can have different magnitudes, and the system can enter topologically protected phases with Chern number $0, \pm 1$. Consequently, the most promising parameter regimes to observe nontrivial topological behaviors lie away from half filling.

We investigate the effect of doping on the edge currents in the bottom panel in Fig. 4. At half filling, the current has a consistent direction along the edge, with a peak at the corners (where two edges meet). At intermediate doping, the current changes direction along the edge, and a small closed loop of current forms at each corner of the system. With further doping, the magnitude of the current along the edge and away from the corners is significantly reduced; however, the small loops of current at the corners of the system remain. Near quarter filling, the current regains a consistent direction, opposite to that at half filling and without the current loops observed at intermediate doping. This behavior is closely connected to the net helicity of the system, which is determined by the occupation of the helicity bands, $\epsilon_{\mathbf{k}}^\pm$. Away from half filling, the occupation of $\epsilon_{\mathbf{k}}^+$ is reduced, resulting in a reduction of the net helicity and consequently a reduction of the edge current. At larger doping, occupation is limited to $\epsilon_{\mathbf{k}}^-$ and the net helicity of the system changes sign, indicated by the change of direction of the current at large doping. The structures in the current are boundary effects of the closed systems. We have verified that in semiperiodic systems the current is essentially constant along the edge but shows the same trend in the dependence of the magnitude and sign on doping.

These observations leave open the intriguing question of how the supersolid state we have characterized evolves as a function of spin imbalance and doping. For spin-imbalanced lattice fermions without SOC, the system supports finite-momentum pairing states, which is seen directly in Hartree-Fock-Bogoliubov-type calculations [44] and can be inferred, via particle-hole symmetry, from more rigorous many-body results on the doped repulsive Hubbard model, which is predicted by AFQMC and other calculations [45,46] to support spin-density waves. Exactly how these Fulde-Ferrell-Larkin-Ovchinnikov-type pairing states compete or coexist with possible Majorana modes in the presence of SOC is a question deserving of careful further numerical investigation. Because of broken time-reversal symmetry, the sign problem will reemerge but can be systematically controlled using the constrained-path AFQMC technique [47].

In summary, we have presented the first numerically exact precision many-body study of a system directly realizable by ultracold atom experiments in an optical lattice with an artificial gauge field. The system exhibits

exotic properties, with a supersolid phase containing both singlet and triplet pairing, and topological signatures in the form of edge currents from SOC. Using state-of-the-art quantum Monte Carlo simulations, we have provided a full, unbiased treatment of the many-body Schrödinger equation to reliably characterize the effects of strong interactions and their interplay with the band structure and SOC in the ground state. We calculated edge currents, which provide a fingerprint for the presence of topological behavior and are a possible precursor of Majorana edge modes when the parameter space of this system is further tuned and scanned.

This research was supported by National Science Foundation (NSF) (Grant No. DMR-1409510), and the Simons Foundation. Computing was carried out at the Extreme Science and Engineering Discovery Environment (XSEDE), which is supported by NSF Grant No. ACI-1053575, and the computational facilities at the College of William and Mary.

-
- [1] I. Bloch, J. Dalibard, and W. Zwerger, *Rev. Mod. Phys.* **80**, 885 (2008).
- [2] M. Lewenstein, A. Sanpera, V. Ahufinger, B. Damski, A. Sen(De), and U. Sen, *Adv. Phys.* **56**, 243 (2007).
- [3] D. Jaksch and P. Zoller, *New J. Phys.* **5**, 56 (2003).
- [4] K. Osterloh, M. Baig, L. Santos, P. Zoller, and M. Lewenstein, *Phys. Rev. Lett.* **95**, 010403 (2005).
- [5] K. Jiménez-García, L. J. LeBlanc, R. A. Williams, M. C. Beeler, A. R. Perry, and I. B. Spielman, *Phys. Rev. Lett.* **108**, 225303 (2012).
- [6] M. Aidelsburger, M. Atala, S. Nascimbène, S. Trotzky, Y.-A. Chen, and I. Bloch, *Phys. Rev. Lett.* **107**, 255301 (2011).
- [7] H. Miyake, G. A. Siviloglou, C. J. Kennedy, W. C. Burton, and W. Ketterle, *Phys. Rev. Lett.* **111**, 185302 (2013).
- [8] F. Gerbier and J. Dalibard, *New J. Phys.* **12**, 033007 (2010).
- [9] J. Alicea, *Rep. Prog. Phys.* **75**, 076501 (2012).
- [10] C. Nayak, S. H. Simon, A. Stern, M. Freedman, and S. Das Sarma, *Rev. Mod. Phys.* **80**, 1083 (2008).
- [11] J. D. Sau, R. M. Lutchyn, S. Tewari, and S. Das Sarma, *Phys. Rev. Lett.* **104**, 040502 (2010).
- [12] L. W. Cheuk, M. A. Nichols, K. R. Lawrence, M. Okan, H. Zhang, and M. W. Zwierlein, *Phys. Rev. Lett.* **116**, 235301 (2016).
- [13] D. Greif, M. F. Parsons, A. Mazurenko, C. S. Chiu, S. Blatt, F. Huber, G. Ji, and M. Greiner, *Science* **351**, 953 (2016).
- [14] L. W. Cheuk, M. A. Nichols, M. Okan, T. Gersdorf, V. V. Ramasesh, W. S. Bakr, T. Lompe, and M. W. Zwierlein, *Phys. Rev. Lett.* **114**, 193001 (2015).
- [15] E. Haller, J. Hudson, A. Kelly, D. A. Cotta, B. Peaudecerf, G. D. Bruce, and S. Kuhr, *Nat. Phys.* **11**, 738 (2015).
- [16] M. F. Parsons, F. Huber, A. Mazurenko, C. S. Chiu, W. Setiawan, K. Wooley-Brown, S. Blatt, and M. Greiner, *Phys. Rev. Lett.* **114**, 213002 (2015).
- [17] J. Radić, A. Di Ciolo, K. Sun, and V. Galitski, *Phys. Rev. Lett.* **109**, 085303 (2012).
- [18] H.-K. Tang, X. Yang, J. Sun, and H.-Q. Lin, *Europhys. Lett.* **107**, 40003 (2014).
- [19] X. Zhang, W. Wu, G. Li, L. Wen, Q. Sun, and A.-C. Ji, *New J. Phys.* **17**, 073036 (2015).
- [20] Q. Sun, G.-B. Zhu, W.-M. Liu, and A.-C. Ji, *Phys. Rev. A* **88**, 063637 (2013).
- [21] W. S. Cole, S. Zhang, A. Paramekanti, and N. Trivedi, *Phys. Rev. Lett.* **109**, 085302 (2012).
- [22] M. Iskin, *Phys. Rev. A* **88**, 013631 (2013).
- [23] Y. Xu, C. Qu, M. Gong, and C. Zhang, *Phys. Rev. A* **89**, 013607 (2014).
- [24] S. Zhang, in *Emergent Phenomena in Correlated Matter: Modeling and Simulation*, edited by E. Pavarini, E. Koch, and U. Schollwöck (Verlag des Forschungszentrum Jülich, Jülich, Germany, 2013), Vol. 3.
- [25] F. F. Assaad, in *Quantum Simulations of Complex Many-Body Systems: From Theory to Algorithms*, edited by J. Grotendorst, D. Marx, and A. Muramatsu (NIC, Jülich, Germany, 2002), Vol. 10, pp. 99–156.
- [26] G. Sugiyama and S. Koonin, *Ann. Phys. (N.Y.)* **168**, 1 (1986).
- [27] H. Shi, S. Chiesa, and S. Zhang, *Phys. Rev. A* **92**, 033603 (2015).
- [28] S. Zhang and H. Krakauer, *Phys. Rev. Lett.* **90**, 136401 (2003).
- [29] H. Shi and S. Zhang, *Phys. Rev. E* **93**, 033303 (2016).
- [30] H. Shi, P. Rosenberg, S. Chiesa, and S. Zhang, *Phys. Rev. Lett.* **117**, 040401 (2016).
- [31] See Supplemental Material at <http://link.aps.org/supplemental/10.1103/PhysRevLett.119.265301> for (a) a description of the computational method and (b) a comparison of AFQMC and mean-field results for density-density and pair-pair correlations. Also included are additional Refs. [32–34].
- [32] P. Rosenberg, H. Shi, and S. Zhang, arXiv:1710.00887.
- [33] J. E. Hirsch, *Phys. Rev. B* **28**, 4059 (1983).
- [34] W. Purwanto and S. Zhang, *Phys. Rev. E* **70**, 056702 (2004).
- [35] Z. C. Wei, C. Wu, Y. Li, S. Zhang, and T. Xiang, *Phys. Rev. Lett.* **116**, 250601 (2016).
- [36] G. V. Chester, *Phys. Rev. A* **2**, 256 (1970).
- [37] A. Andreev and I. Lifshitz, *Sov. Phys. JETP* **29**, 1107 (1969).
- [38] A. J. Leggett, *Phys. Rev. Lett.* **25**, 1543 (1970).
- [39] R. T. Scalettar, E. Y. Loh, J. E. Gubernatis, A. Moreo, S. R. White, D. J. Scalapino, R. L. Sugar, and E. Dagotto, *Phys. Rev. Lett.* **62**, 1407 (1989).
- [40] A. Moreo and D. J. Scalapino, *Phys. Rev. Lett.* **66**, 946 (1991).
- [41] C. N. Yang, *Rev. Mod. Phys.* **34**, 694 (1962).
- [42] S. L. Goertzen, K. Tanaka, and Y. Nagai, *Phys. Rev. B* **95**, 064509 (2017).
- [43] A. Kubasiak, P. Massignan, and M. Lewenstein, *Europhys. Lett.* **92**, 46004 (2010).
- [44] S. Chiesa and S. Zhang, *Phys. Rev. A* **88**, 043624 (2013).
- [45] C.-C. Chang and S. Zhang, *Phys. Rev. Lett.* **104**, 116402 (2010).
- [46] B.-X. Zheng, C.-M. Chung, P. Corboz, G. Ehlers, M.-P. Qin, R. M. Noack, H. Shi, S. R. White, S. Zhang, and G. Kin-Lic Chan, *Science* **358**, 1155 (2017).
- [47] S. Zhang, J. Carlson, and J. E. Gubernatis, *Phys. Rev. B* **55**, 7464 (1997).